Title: Continuous Synthesis of Zn_2Al-CO_3 Layered Double Hydroxides for the Adsorption of Reactive Dyes from Water

Author: Ian Clark Jacob Smith Rachel L. Gomes Edward Lester

PII: S2213-3437(19)30298-2
DOI: https://doi.org/doi:10.1016/j.jece.2019.103175
Reference: JECE 103175

To appear in:

Received date: 12 November 2018
Revised date: 8 May 2019
Accepted date: 24 May 2019

Please cite this article as: I. Clark, J. Smith, R.L. Gomes, E. Lester, Continuous Synthesis of Zn_2Al-CO_3 Layered Double Hydroxides for the Adsorption of Reactive Dyes from Water, *Journal of Environmental Chemical Engineering* (2019), https://doi.org/10.1016/j.jece.2019.103175

Highlights

- Calcined LDH (MMO) exhibits greater adsorption capacity than activated carbons
- Evidence that dyes intercalate into interlayer region of regenerated LDH
- RO16 undergoes higher adsorption than RB5 due to dye structure
- Regeneration mechanism elucidated showing a 'memory mechanism'

Continuous Synthesis of Zn_2Al-CO_3 Layered Double Hydroxides for the Adsorption of Reactive Dyes from Water

[a, b]Ian Clark, [a, b]Jacob Smith, [b]Rachel L. Gomes, [a]Edward Lester

[a]Advanced Materials Research Group, Faculty of Engineering, University of Nottingham, Nottingham, NG7 2RD, United Kingdom

[b]Food, Water, Waste Research Group, Faculty of Engineering, University of Nottingham, Nottingham, NG7 2RD, United Kingdom

Abstract

A novel pilot scale approach to continuous synthesis of layered double hydroxides (LDHs) was used to produce Zn_2Al-CO_3. The Zn_2Al-CO_3 was calcined and used in the adsorption of Reactive Black 5 (RB5) and Reactive Orange 16 (RO16) from water. The specific surface area of the LDH was 50.1 m^2 g^{-1}, while the surface area of the calcined LDH (MMO) was 57.8 m^2 g^{-1}. X-ray diffraction indicated complete breakdown of the LDH at 500°C for 4 hours, with amorphous Al_2O_3 or AlOOH alongside ZnO. Reaction variables in the adsorption system; temperature, adsorbent dose, pH, initial concentration and the effect of competing anions were investigated across four temperatures from 10°C to 40°C. Maximum adsorption capacity calculated from the Langmuir isotherm was 895 mg g^{-1} and 589 mg g^{-1} at 20°C, for RB5 and RO16, respectively. Intercalation of dye molecules was the main mode of adsorption, as indicated by shifts in (*003*) reflection from 11.5° to 4.5° and 3.2° for RB5 and RO16 respectively. Adsorption was best modelled by the pseudo 2nd order kinetic model. The intra-particle diffusion model indicated multiple stages of adsorption; surface adsorption occurs initially, followed by,

intra-particle diffusion of dye molecules into the interlayer region. Regeneration through calcination resulted in an adsorption equal to 99±2%.

Keywords

Continuous Flow Synthesis; Layered Double Hydroxides; Reactive Dyes; Adsorption Kinetics; Thermodynamics

1. Introduction

Textile manufacture and dyeing is a global industry, with synthetic dyes dominating the textile industry. The most common type synthetic dye is the azo dye, so named since at least one azo (R'-N=N-R') functional group is present in the chemical structure. Azo dyes account for up to 70% of all synthetic dyes [1-3]. Reactive dyes are most typically applied to cellulose substrates and are prevalent in the textiles industry [4]. Although reactive dyes benefit from covalent bonding to the substrate resulting in good wash and light fastness, they can hydrolyse under prolonged exposure to highly alkaline conditions. Dye hydrolysis can result in fixation rates as low as 60% [1]. Many synthetic dyes are stable and recalcitrant in natural environments, and biological wastewater remediation such as activated sludge processes do not perform well when removing these dyes [5].Layered double hydroxides (LDHs) have been utilised for dye remediation . LDHs are a range of synthetic anionic clay minerals that follow the chemical formula $[M^{II}_{1-x}M^{III}_{x}(OH)_2](A^{n-})_{x/n}\cdot zH_2O$. M^{II} and M^{III} are representative of cationic species (Mg^{2+}, Ca^{2+}, Zn^{2+}, Al^{3+}, Cr^{3+}) while A^{n-} is representative of interlayer anions that hold the M^{II} and M^{III} hydroxide layers together through electrostatic attractions [6, 7]. A characteristic of LDHs, known as the *memory effect* enables them to be utilised for adsorption. The

memory effect works by heating the LDH to a critical temperature that results in evolution of the interlayer anion and dehydroxylation of the brucite like layers; rehydrating the resulting mixed metal oxide (MMO) in the presence of anionic species causes the LDH to reform with the anionic compound present in the interlayer region [8, 9]. The temperature of calcination is important as overheating the LDH will result in spinel structures forming that cannot undergo rehydration [10], while under-heating will result in an incomplete degradation of the layered structure and the full capacity of the MMO will not be achieved. The memory effect for MMO/LDH adsorption was first exploited in the adsorption of halide ions such as fluoride and bromide as well as heavy metal oxoanionic compounds that are typically found in wastewaters [11-14]. More recently however, the capability of LDHs and MMOs as dye adsorbents has been studied. The most extensive area of research into dye adsorption onto MMO/LDH adsorbents has been focussed on acidic dyes with methyl orange, possibly due to its inherent toxicity, being a recurring pollutant of interest [15-18]. Nevertheless, there is a substantial number of LDHs and an even greater range of synthetic dyes [19-22] so more work is needed in this area to establish LDH based adsorbents as a means of removing and recovering dyes from wastewater streams. The work in this research aims to utilise a more novel approach of large scale continuous synthesis of Zn_2Al-CO_3 LDHs and its application as an adsorbent for Reactive dyes which, to the knowledge of the authors, have yet to be investigated.

2. Experimental Section

2.1. Materials

All chemicals were used as received without further purification. Zinc nitrate hexahydrate (>98%), aluminium nitrate nonahydrate (>98%), sodium hydroxide (>98%), sodium

carbonate (>98%), Reactive Black 5 (RB5) (≥50%), Reactive Orange (RO16) (≥70%) were purchased from Sigma Aldrich (Devon, UK). These dye compounds exhibit differences in terms of size and chemical structure (Figure 1). Sodium sulfate (>98%) was obtained from Fisher Scientific (Leicestershire, UK). Prior to experimentation all relevant solutions were prepared fresh with deionised water.

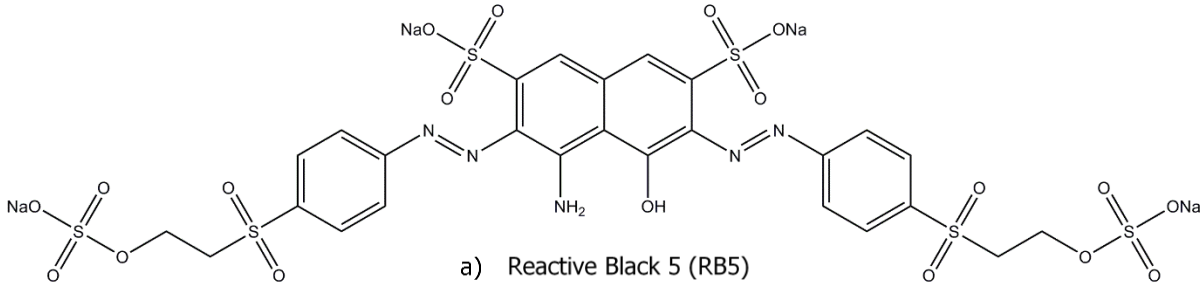

a) Reactive Black 5 (RB5)

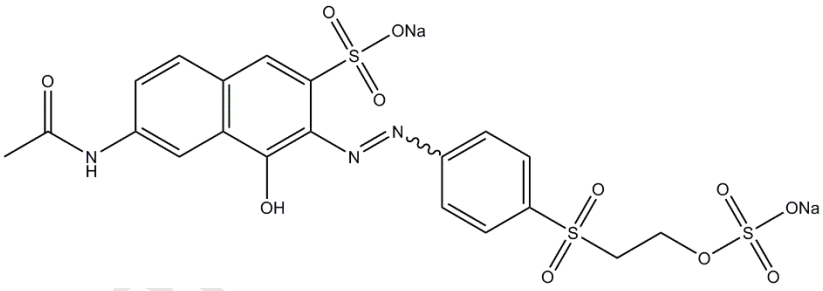

b) Reactive Orange 16 (RO16)

Figure 1 Structure of Reactive dyes a) Reactive Black 5 (RB5) b) Reactive Orange 16 (RO16)

2.2. Layered Double Hydroxide and Mixed Metal Oxide Synthesis and Characterisation

Zn_2Al-CO_3 was produced using a counter-current flow in a process similar to that reported by Clark *et al.* [23]. However, the scale of the synthesis was increased by a factor of approximately 20 from bench to pilot scale. Briefly a solution of $Zn(NO_3)_2$ (0.067 mol L^{-1})

and $Al(NO_3)_3$ (0.033 mol L^{-1}) was pumped into the reactor via the up-flow feed at 200 mL min^{-1}, while a solution consisting of NaOH (0.125 mol L^{-1}) and Na_2CO_3 (0.0167 mol L^{-1}) was pumped at 400 mL min^{-1} via the down-flow feed into the reactor. The reactor was comprised of Swagelock® 316 stainless steel tubing and fittings and pressure was maintained in the system at 24 MPa by a back-pressure regulator (Pressure Tech, UK). Following synthesis the wet product was allowed to settle, and the concentrated suspension was washed by centrifugation with deionised water and freeze dried. X-ray diffraction was carried out on a Bruker D8-Advance diffractometer with Cu Kα radiation (λ=1.5418 nm) in a Bragg angle range of 2-70°, 2θ and a slit width of 6mm. Surface area and pore size distribution were calculated from nitrogen adsorption isotherms. Nitrogen adsorption was carried out using a Micromeritics Tristar II 3020 at -196°C. Samples were outgassed at 105°C for 24 hours prior to analysis. Thermal stability of LDH powders and water content was analysed using thermogravimetric analysis carried out on a TA Q500 thermogravimetric furnace in N_2 atmosphere (Flowrate = 40 mL min^{-1}) up to 700°C. TEM analysis was performed on a JEOL 2100F TEM with a LaB_6 filament and an acceleration voltage of 200 kV. Samples were dispersed in and dropped onto lacy carbon films on 300 mesh copper grids (Agar Scientific). Images were captured using a Gatan Orius digital camera. To prepare the LDH for adsorption experiments, the freeze-dried powder was calcined in air at 500°C for 4 hours and labelled MMO.

2.3. MMO Stability in Air and Water

Samples of freshly calcined MMO were placed in storage at room temperature (291±2 K) in the dark in sealed vials. Samples were stored in deionised water to establish the effects of water on the crystal structure of the MMO and any detectable memory effect, during term use. Dry stored samples were investigated to establish the effects of storage of the MMO adsorbent. Samples were removed from storage every 2 weeks, for 8 weeks and

analysed using X-ray diffraction to identify any changes to the crystal structure. Prior to analysis, wet stored samples were freeze dried in the same way as freshly synthesised LDH was prepared for characterisation.

2.4. Adsorption Experiments

Batch adsorption experiments were carried out in an incubator with magnetic stirring for agitation. The effect of temperature, initial dye concentration, adsorbent dose, initial pH, coexisting anions were all investigated as was the recycling and regeneration of the MMO. Typically, 50 ml of RB5 or RO16 solution and 1 g L^{-1} of MMO were used in 250 mL conical flasks. After adsorption, liquid aliquots were taken and centrifuged. The supernatant was then analysed using a Shimadzu UV-mini 1240 spectrophotometer at the λ_{max} for RB5 (λ_{max}=597 nm) and RO16 (λ_{max}=388 nm). Uptake of dye was calculated from the following equation (eq.1) [24]:

$$q=\frac{(C_0-C)\times V}{m} \quad (1)$$

Where q (mg g^{-1}) is the uptake, C_0 is the initial dye concentration and C is the sample dye concentration (mg L^{-1}) a given time (C_t) or at equilibrium (C_e), V is the volume of the dye solution (L) and m is the mass of the adsorbent (g).

For experiments investigating the effect of temperature, aliquots were taken at predetermined time intervals until equilibrium was reached. Experiments investigating the effect initial dye concentration samples were allowed to reach equilibrium before aliquots were taken for analysis. Initial dye concentration was adjusted between 100 and 1500 mg L^{-1}. Following analysis, the exhausted adsorbent was isolated from the supernatant, washed to remove any residual dye and freeze dried. The freeze-dried adsorbent was the analysed using XRD to establish changes in the interlayer region to determine if

intercalation or surface adsorption has occurred. High temperatures, can be used to increase fixation of dyes onto substrates [4]. The effect of temperature was investigated at an adsorbent dose of 1 g L^{-1} and initial dye concentration of 1500 mg L^{-1}. Temperature was varied from 10°C to 40°C. Solutions were stirred and samples were taken and analysed every 15 minutes until equilibrium was reached, which was typically between two and three hours.

2.5. Effect of Adsorbent Dose

Dye concentration were maintained at 1500 mg L^{-1} of dye and 20°C. Adsorbent dose was set at 0.5 g L^{-1}, 1 g L^{-1}, 1.5 g L^{-1} and 2g L^{-1}. Samples were analysed at given time intervals to evaluate the effect that adsorbent dose has on the uptake of dye over time.

2.6. Effect of Initial pH

High pH, can increase fixation of reactive dyes onto cellulose substrates [4].The effect of initial pH was assessed at an adsorbent dose of 1 g L^{-1} and initial dye concentration of 1500 mg L^{-1}. Temperature was maintained at 20°C. Solution pH was adjusted using HCl and NaOH. Solutions were stirred until equilibrium was reached before samples were analysed.

2.7. Effect of Competing Anions

Electrolyte addition and addition of alkaline chemicals to dye baths can also promote dye diffusion fixation and in the substrate [4]. Solutions of dye at 1500 mg L^{-1} were prepared with coexisting anions at concentrations between 0 to 10000 mg L^{-1}. The co-existing anions (CO_3^{2-}, SO_4^{2-} and Cl^-) were prepared in the same solution with the dyes, at varying concentration, from their respective sodium salts. The samples were stirred at 20°C, with

1 g L^{-1} of adsorbent, until equilibrium was reached. Samples were then analysed using UV-Vis spectrophotometry.

2.8. Adsorbent Regeneration

Regeneration and recyclability of exhausted adsorbents is a key characteristic that enhances sustainability of the adsorption process. A solution of RB5 (1500 mg L^{-1}) was stirred at 20°C with 1 g L^{-1} of adsorbent until equilibrium was reached. From here two post adsorption regeneration methods were investigated. After analysis the exhausted adsorbent washed with water to remove any residual dye. The samples were then calcined at 500°C for 4 hours as the generation of the MMO was carried out at this temperature. This resulting powder was reused in the next adsorption cycle. The process was followed for 4 cycles. An alternative to this method involved washing with Na_2CO_3 to remove and recover the adsorbed dye. The adsorbent was then calcined at 500°C for 4 hours and re-used in adsorption experiments.

3. Results and Discussion

3.1. Adsorbent LDH and MMO Crystal Characteristics

The diffractograms for LDH and MMO samples are detailed in Figure 2. Intense symmetric basal reflections for Zn_2Al-CO_3 are clearly defined in the diffractogram at 11.5° and 23.2° relating to (*003*) and (*006*) respectively. LDH exhibits hexagonal crystal symmetry in a rhombohedral setting with space group $R\bar{3}m$ [25]. Lattice parameters were calculated as 0.31 nm and 2.29 nm for *a* and *c* respectively. Crystal domain length (CDL) calculated using the full width at half maximum (FWHM) of the (*003*) and (*110*) reflections and the Scherrer equation. CDL of the LDH was calculated as 26 nm in the ⟨*003*⟩ plane and 50 nm in the ⟨*110*⟩ plane. The diffractogram for the MMO sample shows reduced intensity of reflections and the only observable reflections in the pattern pertain to ZnO as evidenced

by reflections at 31.8°, 34.5° and 36.3° relating to (*010*), (*002*) and (*011*) respectively. This could indicate that the AlOOH and Al_2O_3 present in the sample were amorphous, suggesting a mixture of metal oxides formed as opposed to a singular MMO. However, no data was found in the Inorganic Crystal Structure Database (ICSD) that attributes to the crystalline structure of MMO expected. Upon heating the LDH loses surface bound and interlayer water. The LDH then undergoes dehydroxylation of the brucite-like layers and then the interlayer CO_3^{2-} is evolved as CO_2[17]. There are no visible reflections relating to the LDH or spinel $ZnAl_2O_4$ structures. Lattice parameters for the ZnO in the MMO sample were calculated as 0.32 nm and 0.52 nm for *a* and *c* respectively, which is in agreement with literature [26].

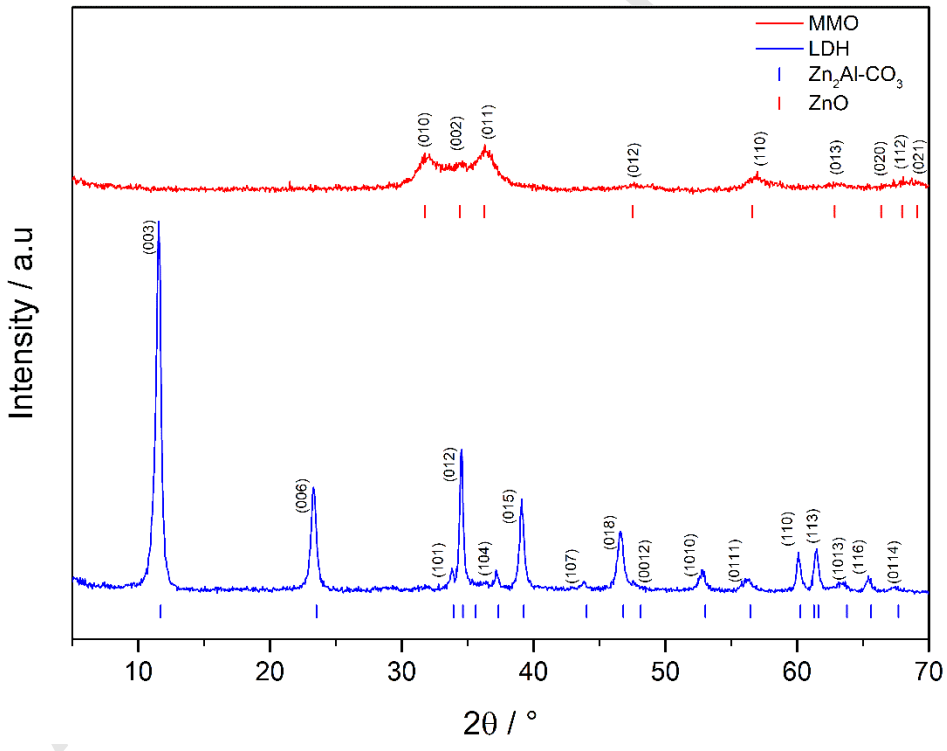

Figure 2 Diffractogram of Zn_2Al-CO_3 samples, before (LDH) and after (MMO) calcination

3.2. Stability of MMO in water

Prolonged storage of MMO samples in deionised water resulted in the rehydration of the MMO and reformation of the Zn_2Al-CO_3 LDH (Figure 3). The reformation of the LDH was

slow and the increasing crystallinity with increasing storage time suggests that use with primarily low concentrations of contaminant dyes or excessive washing with clean water will result in reductions in adsorption as the alkalinity of reforming LDH layers causes increased absorption and adsorption of CO_2 and CO_3^{2-} respectively [27]. Despite the reformation of the LDH to a large extent, within the samples there are reflections present at 32° and 36° relating to the (*010*) and (*011*) reflections of ZnO. This is a result of some irreversible ZnO formation during calcination. The regenerated samples after 6 and 8 weeks of storage show relative reflection intensity that is comparable to the fresh LDH, and each other. This suggests that further regeneration is unlikely to occur with further storage.

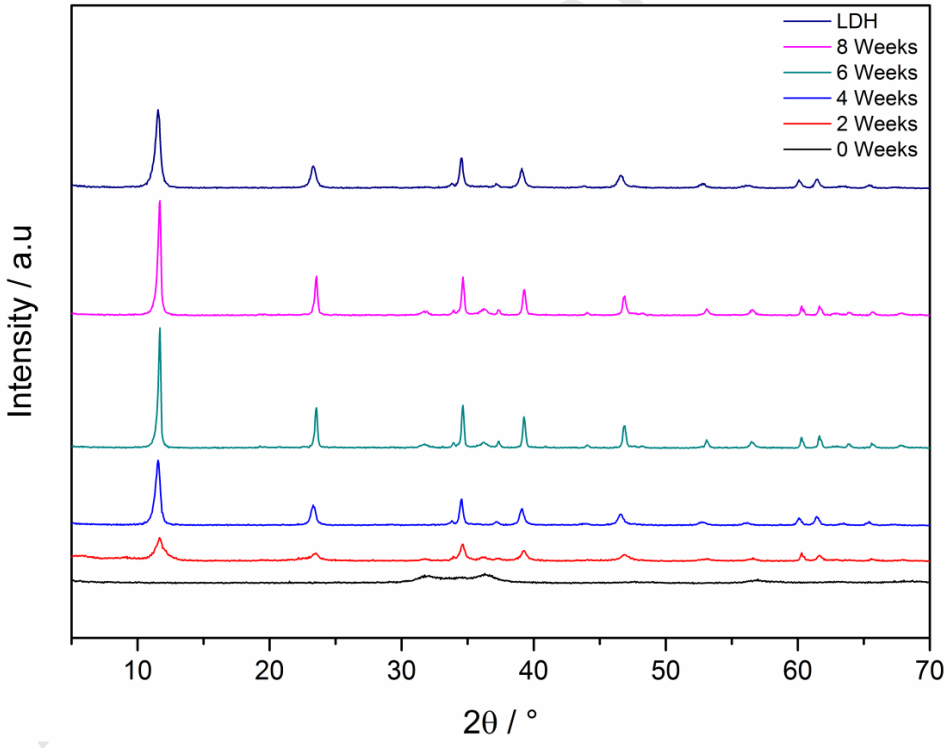

Figure 3 Changes in diffraction patterns and crystal structures of mixed metal oxide during wet storage

3.3. Surface Area and Pore Size Analysis

Surface area is usually a key characteristic in adsorption, with high surface area a desired trait in a material. Nitrogen adsorption isotherms of both the LDH and MMO exhibit a Type-IV shape which suggests mesopores are present within the materials (Figure 4). The adsorption branch of a Type-IV isotherm resembles a Type-II isotherm and shows that there is mono and multilayer adsorption on pore walls up to high relative pressures (P/P_0, whereby P and P_0 are equilibrium and saturation pressures respectively), which is followed by condensation in the mesopores. The hysteresis most closely resembles H3 hysteresis (according to IUPAC classifications), there is not significant plateau at the highest point on either the adsorption or desorption branches of the isotherm. This indicates that the gas adsorption was occurring between loosely packed agglomerates of platelet like particles [28] which is supported by the layered structure of the LDH and MMO materials detailed in (Figure 4). The slight increase in surface area (S_{BET}) and decrease in pore diameter between the LDH and MMO (Table 1) is attributed to increased access to smaller pores in the agglomerates post calcination with the break-down of the strict layered structure of the LDH. Increased specific surface area of MMO samples compared to LDH samples is common in adsorption research [29-31].

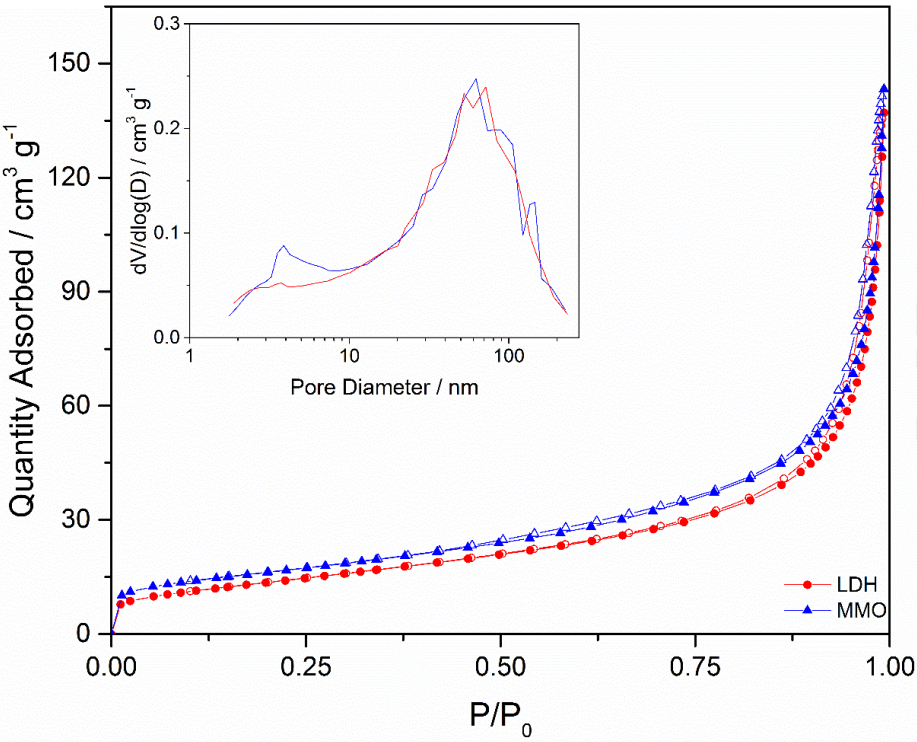

Figure 4 Nitrogen adsorption isotherm for Zn_2Al-CO_3 (LDH) and calcined Zn_2Al-CO_3 (MMO).

Inset; pore size distribution calculated from the desorption branch of the isotherm

Table 1 Specific surface area and pore diameter of LDH and MMO

Sample	S_{BET} / m^2 g^{-1}	Desorption BJH Pore Average Diameter / nm
LDH	50.1 ± 0.2	15.3
MMO	57.8 ± 0.1	14.1

3.4. Effect of initial pH on Adsorption

Alkaline conditions, along with high temperature, is ideal for fixation of reactive dyes onto cellulose substrates [3, 4]. Despite this, the effect of pH from 4-10 is shown to have little

impact on the adsorption of dyes onto LDH (Figure 5), as evidenced by the mean q_e of RO16 remaining constant between 700 and 800 mg g^{-1}. However, the mean q_e of RB5 was lower at 500-600 mg g^{-1}. The reduced adsorption capacity of the MMO for RB5 compared to RO16 is most likely due to increased steric hindrance of RB5 due to its bulkier size and the greater number of R-SO_3^- functional groups in the molecule, which occupy a greater number of active sites on the LDH surface. Adsorption under increasingly acidic conditions will diminish due to the dissolution of the MMO/LDH structure [31]. Adsorption under increasingly alkaline conditions could also diminish due to Zn^{2+} and Al^{3+} dissolving into zincate and aluminate. The adsorbent however, does remain stable at pH 4 and further reduction in pH is unlikely to occur due to the addition of alkaline chemicals in the dyeing processes [3]. The implication of this data is that MMO adsorbents exhibit comparable performance across a wide pH range, thus pH modification would not be necessary prior to adsorption.

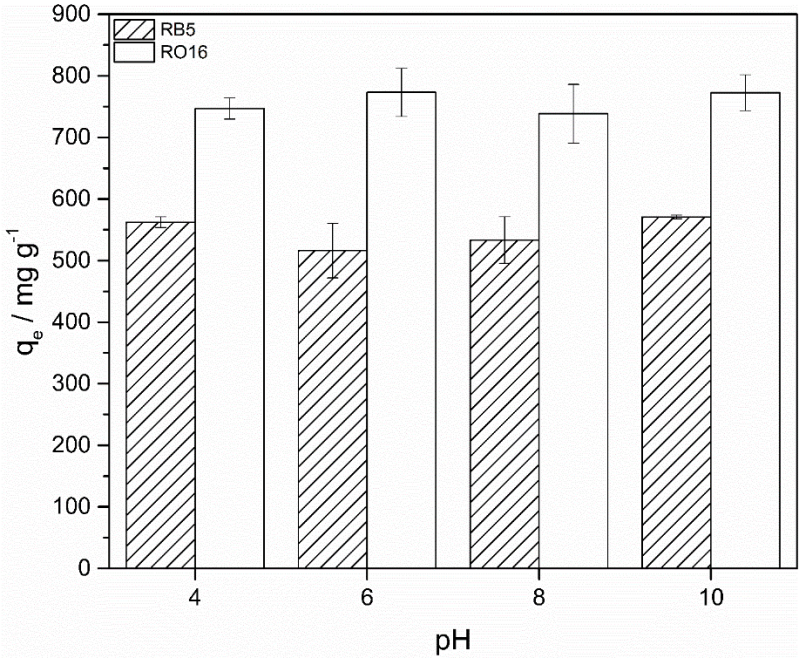

Figure 5 Effect of pH on adsorption of Reactive Black 5 (RB5) and Reactive Orange 16 (RO16) from simulated wastewater (C_0=1500 mg L^{-1}; V_{dye}=50 mL; adsorbent loading=1 g L^{-1}; T=20°C)

3.5. Effect of Adsorbent Dose

The adsorbent dose experiments for adsorption of RB5 (Figure 6a) indicate that there is a small change in overall uptake, however the rate of uptake remains relatively constant across adsorbent loading from 0.5-2 g L^{-1}. Final adsorbate concentration (C_e) decreases with increasing adsorbent loading. The reduction in C_e is close to 250 mg L^{-1} per 0.5 g L^{-1} increase in adsorbent loading. Adsorbent loading in RO16 adsorption is more variable (Figure 6b). Equilibrium uptake (q_e) varies from 589 mg g^{-1} with 0.5 g L^{-1} to 867 mg g^{-1} with 1g L^{-1}. Equilibrium concentration is reduced with more variation compared with RB5. C_e is reduced from 1104 mg L^{-1} (adsorbent loading at 0.5 g L^{-1}) to 604 mg L^{-1} (adsorbent loading at 1 g L^{-1}). The change in C_e from 1 g L^{-1} to 2 g L^{-1} is more constant, being on average 270 mg L^{-1}. The data from the adsorption of RB5 indicates that the adsorbent loading can be increased in adsorption processes compared to RO16 due to the higher q_e when adsorbing aqueous RO16 from solution. However adsorbent loading of approximately 2 g L^{-1} leads to inefficient adsorption as some MMO is left unsaturated. This may also have further implications when looking into the regeneration and increased buffering effect of LDH layers. The presence of unsaturated MMO will adsorb water and dissolved CO_2 to reform carbonate intercalated LDH, which can further increase the buffering effect and lead to great levels of CO_2 absorption and increase the potential of CO_3^{2-} intrusion into the LDH layers, thus reducing the effective adsorption capacity of the MMO. It therefore appears that adsorbent loading of 1-1.5 g L^{-1} is optimum for adsorption of RB5 and RO16.

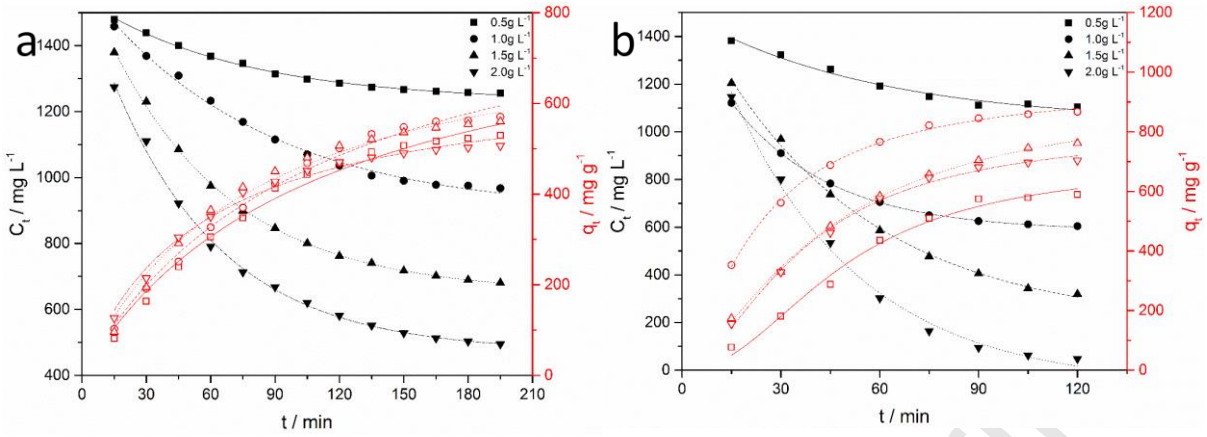

Figure 6 Effect of adsorbent dose on adsorption of a) Reactive Black 5 b) Reactive Orange 16 from simulated wastewater (C_0=1500 mg L^{-1}; V_{dye}=50 mL; adsorbent loading=1 g L^{-1}; T=20°C)

3.6. Adsorption Isotherms

Isotherm characteristics of adsorption of RB5 and RO16 on Zn_2Al MMO were modelled using the Langmuir and Freundlich isotherm models. The Langmuir isotherm model can be described in a non-linear (eq.2) and linear (eq.3) form [32]:

$$q_e = \frac{q_m k_l C_e}{1 + k_l C_e} \quad (2)$$

$$\frac{C_e}{q_e} = \frac{C_e}{q_m} + \frac{1}{k_l q_m} \quad (3)$$

Where k_l (L mg^{-1}) is the Langmuir constant, q_m (mg g^{-1}) and q_e (mg g^{-1}) are the maximum uptake capacity and the equilibrium uptake capacity, respectively, C_e (mg L^{-1}) is the equilibrium adsorbate concentration. The non-linear (eq.4) and linear (eq.5) forms of the Freundlich isotherm can be described as [32]:

$$q_e = k_f C_e^{\frac{1}{n}} \quad (4)$$

$$\ln(q_e) = \ln(k_f) + \frac{1}{n}\ln(C_e) \quad (5)$$

Where k_f (mg g^{-1}.(L $mg^{-1})^{1/n}$) is the Freundlich isotherm constant and 1/n is the heterogeneity factor. The Langmuir and Freundlich models for RB5 and RO16 are illustrated in Figure 7 and Figure 8 respectively. The parameters for the Isotherm models are outlined in Table 2. The linear regression fit for both adsorbates decreases with increasing temperature. For both RB5 and RO16, K_l and K_f decrease with temperature suggesting an increased affinity between dye and adsorbent at low temperature and an exothermic nature. The maximum uptake (q_m) for RB5 decreases from 589 mg g^{-1} (20°C) to 544 mg g^{-1} (40°C). The q_m calculated for RO16 increases with increasing temperature over the full experimental range (10°C-40°C). In the case of these temperatures 30°C-40°C, the high q_m calculation comes from the poorer fit of the isotherm model to the data. The Langmuir isotherm fit is poor primarily because, at the higher temperatures, with low C_0, adsorption is inhibited (Figure 7 and Figure 8). The maximum uptake capacity of the MMO for RB5 compared to RO16 is lower in all instances. This is due to the fact that the adsorption of the dye molecules is through the memory effect and regeneration of the LDH from the MMO. RB5 is also bulkier in size and contains four R-SO_3^- functional groups where as RO16 contains only two. The general LDH formula dictates that increasing negative charge of the interlayer anion results in reduced capacity within the interlayer region. The q_m value for temperatures above 30°C fit well with this theory, however surface adsorption to the outer layers of the MMO/LDH adsorbent also occurs which results in the deviation away from an expected ratio of q_m of 2:1 for RO16:RB5. Orthman *et al.* identified a similar trend in the adsorption of acidic blue dyes, where the larger molecules from direct and reactive dyes not adsorbed as well as smaller acidic dyes [33].

Table 2 Isotherm constants

Dye	Temperature / °C	Langmuir			Freundlich		
		k_l / L mg^{-1}	q_m mg g^{-1}	R^2	k_f / mg g^{-1}.(L mg^{-1})$^{1/n}$	n	R^2
RB5	10	0.217	566	0.999	180.92	5.27	0.900
	20	0.076	589	0.998	105.44	3.52	0.639
	30	0.018	550	0.989	28.78	2.20	0.928
	40	0.003	544	0.931	7.68	1.52	0.914
RO16	10	0.089	694	0.997	178.07	4.39	0.707
	20	0.053	895	0.999	122.36	2.84	0.712
	30	0.029	1004	0.973	53.08	1.89	0.641
	40	0.009	1210	0.962	26.94	1.57	0.867

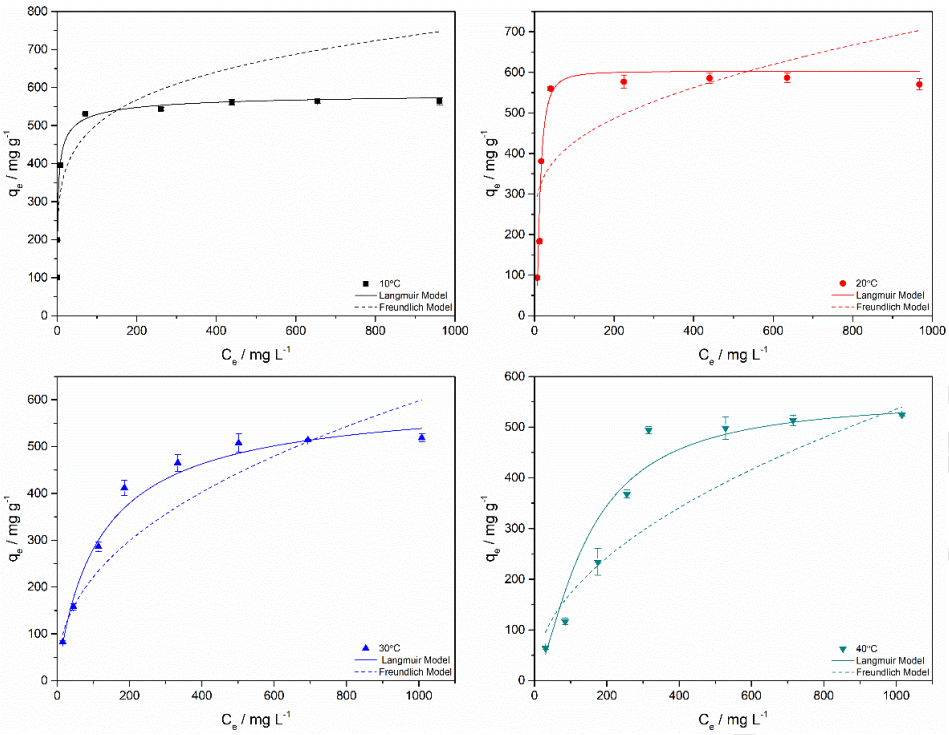

Figure 7 Adsorption Reactive Black 5 from simulated wastewater with variable initial concentration (C_0=100-1500 mg L^{-1}; V_{dye}=50 mL; adsorbent loading=1 g L^{-1})

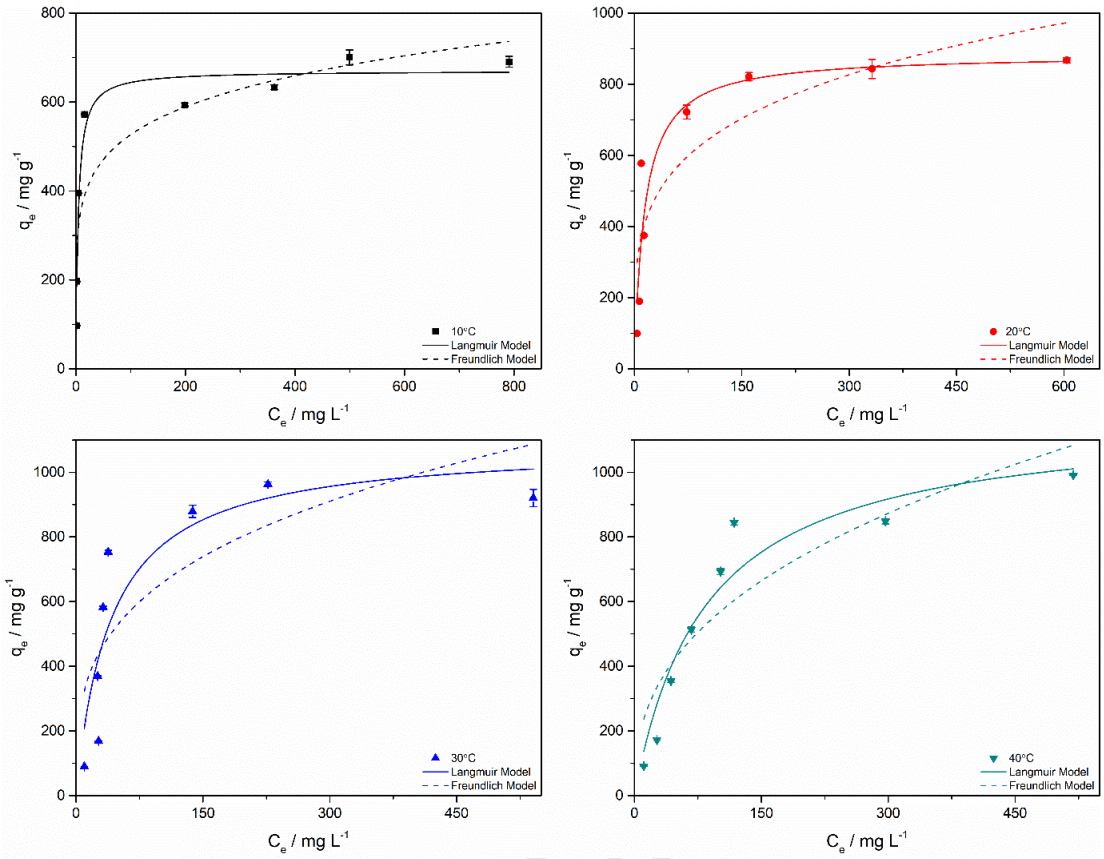

Figure 8 Adsorption Reactive Orange 16 from simulated wastewater with variable initial concentration (C_0=100-1500 mg L^{-1}; V_{dye}=50 mL; adsorbent loading=1 g L^{-1})

The data in Table 3 shows that MMO based adsorbents exhibit a much higher adsorption capacity for RB5 dye compared with other adsorbents that have been investigated [34-41]. Only chitosan exhibited a higher maximum uptake for the dye compared with the MMO adsorbent and many of the reference adsorbents exhibit uptake below 100 mg g^{-1}. This suggests that MMO adsorbents can compete strongly with other adsorbents in terms of capacity for dye uptake and could make them a useful material for dye wastewater remediation.

Table 3 Maximum uptake capacity (q_m) of Reactive Black 5 onto other absorbents

Adsorbent	q_m mg g^{-1}	Reference
Zn_2Al MMO	589	This work
Biomass Fly Ash	4	[34]
Peanut Hull	50	[35]
Aspergillus foetidus	65	[36]
Laminaria sp.	73	[37]
Chlorella vulgaris	476	[38]
Zeolite	64	[39]
Activated carbon (Powdered)	59	[40]
Fly Ash	8	[40]
Chitosan	1100	[41]

3.7. Adsorption Kinetics

The effect of temperature on adsorption can have a profound impact on adsorption kinetics [42]. The data from variable temperature adsorption was fit to three different kinetic models; the pseudo 1st order, pseudo 2nd order and the intra-particle diffusion model. The pseudo 1st order model is expressed in non-linear (eq.6) and linear (eq.7) forms [43] :

$$q_t = q_e\left(1-e^{k_1 t}\right) \quad (6)$$

$$\ln\left(q_e-q_t\right) = \ln\left(q_e\right)-k_1 t \quad (7)$$

Where q_t (mg g^{-1}) and q_e (mg g^{-1}) are the adsorption at time (t; min) and at equilibrium respectively and k_1 (min^{-1}) is the pseudo 1st order rate constant. The pseudo 2nd order model can be expressed in both non-linear (eq.8) and linear (eq.9) forms as follows [43] :

$$q_t = \frac{k_2 q_e^2}{1+k_2 q_e t} \quad (8)$$

$$\frac{t}{q_t} = \frac{1}{k_2 q_e^2} + \frac{t}{q_e} \quad (9)$$

Where k_2 (g mg^{-1} min^{-1}) is the 2nd order rate constant. The third model fitted to the experimental data was the Weber-Morris intra-particle diffusion model (eq.10) [44]:

$$q_t = k_{id}\sqrt{t} + C \quad (10)$$

Where k_{id} is the intra-particle diffusion constant. Plots of the linear pseudo 1st order model for RB5 and RO16 are displayed in 9a and 10a and the kinetic data is outlined in Table 4. From the plots for RB5, adsorption at 10°C and 20°C occurs at similar rate, while adsorption at 30°C and 40°C occurs at increasing rates (9a). RO16 adsorption occurs at similar rates for 20°C and 30°C with adsorption at 10°C and 40°C occurring at much slower and faster rates respectively (Table 4). The fit of the model show an increasing trend with increasing temperature with respect to RB5 adsorption, however this appears to have little influence on the $q_{e,cal}$ for each temperature. For low temperature reactions the $q_{e,cal}$ value is significantly higher than the $q_{e,exp}$ value. The closest $q_{e,cal}$ and $q_{e,exp}$ values occur at 30°C, where the pseudo 1st order model has the poorest fit (R^2=0.818). The trend is also observed in the adsorption of RO16 where again the smallest difference between $q_{e,cal}$ and $q_{e,exp}$ is found at 30°C (Table 4). The pseudo 2nd order rate model is the best fit to the data across all temperatures for adsorption of both RB5 and RO16, as expected from other dyes in literature. [18, 20]. Linear regression analysis indicates a

good fit for temperatures ≥30°C in the adsorption of RB5 and for all temperatures ≥20°C for RO16. The shape of the linear pseudo 2nd order models indicates that at low temperatures early stages of adsorption are slower than the models predict (9b and 10b), this can account for the inferior fit of both RB5 and RO16 at the lowest temperatures (≤20°C). The rate constants for RB5 are similar being that they are close to 7 $x10^{-6}$-$9x10^{-6}$ g mg^{-1} min^{-1} for temperatures 10°C and 20°C. There is an increase, almost in an order of magnitude, when increasing the temperature from 20°C to 30°C. The $q_{e,exp}$ and $q_{e,cal}$ for both RO16 and RB5 grow increasingly close with increasing temperature as does the fit of the models. Suggesting that at higher temperatures the pseudo 2nd order model is the most appropriate. Compared with smaller acidic dyes, such as methyl orange, the reaction rate is several orders of magnitude lower. This indicates that the adsorption of the bulkier reactive dye molecules causes a slower regeneration of the LDH layers [18].

The intra-particle diffusion plots can be separated into three sections for adsorption (Figure 9c and Figure 10c). The first stage of the adsorption is linked to the surface adsorption of the dye molecules onto the surface of the MMO, while the second stage of the adsorption is the migration the adsorbed dye molecules into the interlayer and the resulting regeneration of the LDH. The 3rd stage of adsorption is the reaching of the state of equilibrium in the adsorption system and the adsorbent has become saturated [45]. At higher temperatures the initial stage of surface adsorption occurs more quickly, due to increased molecule energy and increased rate of collisions resulting in adsorption occurring. The second and third stages of diffusion into the interlayer region and reaching equilibrium occur at similar rates between all temperatures tested. The data indicates that, for RB5 adsorption the diffusion of dye into the interlayer region is the rate limiting step in the adsorption reaction [45, 46]. This is also the case for the adsorption of RO16, however at 10°C the surface adsorption of RO16 onto the MMO is the rate limiting step.

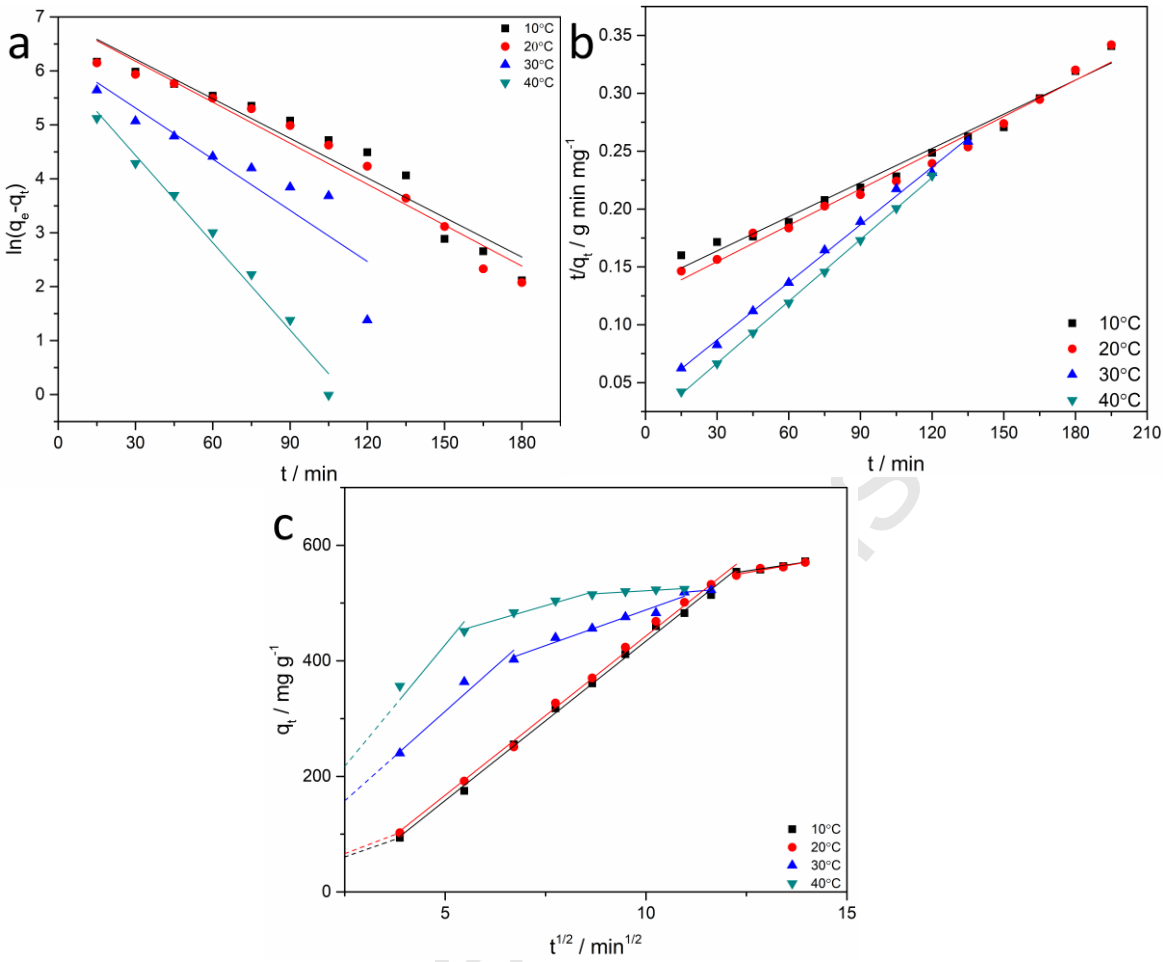

Figure 9 Kinetic models for adsorption of Reactive Black 5 at different temperatures a) Linear pseudo 1st order b) Linear pseudo 2nd order c) Intra-particle diffusion

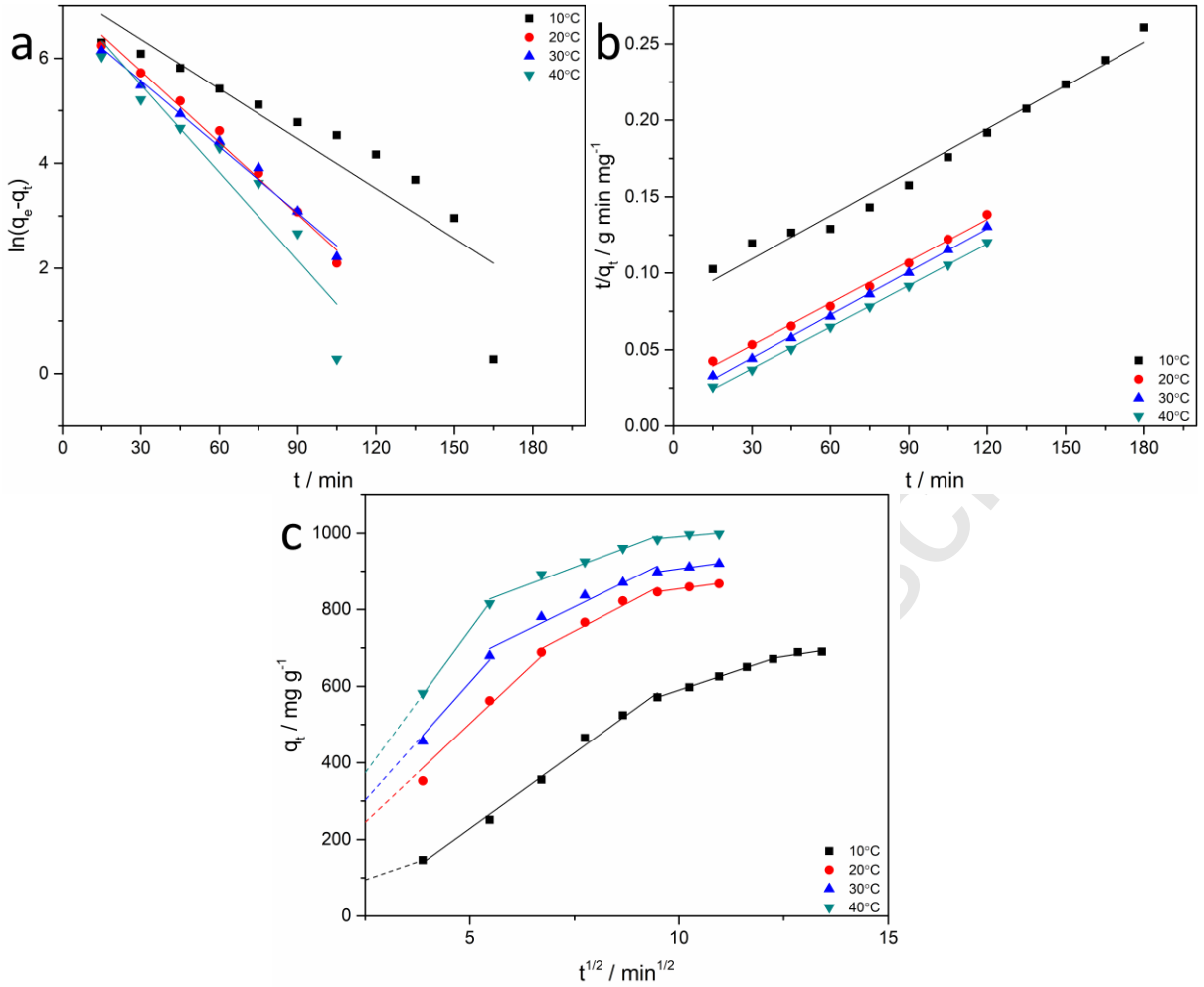

Figure 10 Kinetic models for adsorption of Reactive Orange 16 at different temperatures a) Linear pseudo 1st order b) Linear pseudo 2nd order c) Intra-particle diffusion

Table 4 Reaction rate constants for adsorption of Reactive Black 5 (RB5) and Reactive Orange (RO16) from simulated wastewater

Sample	Temperature / °C	$q_{e,exp}$ / mg g^{-1}	Pseudo 1st order			Pseudo 2nd order		
			k_1 / min^{-1}	$q_{e,cal}$ / mg g^{-1}	R^2	k_2 / g mg $^{-1}$ min^{-1}	$q_{e,cal}$ / mg g^{-1}	R^2
RB5	10	572	0.0245	1046	0.925	$7.211x10^{-6}$	1016	0.981

	20	570	0.0253	1032	0.957	8.949×10^{-6}	952	0.983
	30	523	0.0316	524	0.818	7.434×10^{-5}	602	0.999
	40	542	0.0540	427	0.992	2.377×10^{-4}	562	0.999
RO16	10	690	0.0316	1492	0.829	1.104×10^{-5}	1058	0.982
	20	867	0.0455	1238	0.987	3.269×10^{-5}	1094	0.995
	30	919	0.0419	921	0.917	5.302×10^{-5}	1067	0.999
	40	998	0.0557	1294	0.902	7.760×10^{-5}	1105	0.999

3.8. Adsorption Thermodynamics

The thermodynamic parameters; enthalpy (ΔH) entropy (ΔS) and Gibbs free energy (ΔG) inform on the energy within the system and the spontaneity of the adsorption process. Gibbs free energy can be calculated using two different equations (eq.11 & 12) [24]:

$$\Delta G^\circ = \Delta H^\circ - T\Delta S^\circ \quad (11)$$

$$\Delta G^\circ = -RT\ln k_a \quad (12)$$

Where ΔG (kJ mol^{-1}) is Gibbs free energy, ΔH (kJ mol^{-1}) and ΔS (kJ K^{-1} mol^{-1}) are system enthalpy and entropy respectively, T (K) is the adsorption temperature, R is the gas constant (J K^{-1} mol^{-1}) and k_a is the adsorption coefficient, in this case taken from the Langmuir constant; k_l (L mol^{-1}). Combining the equations for Gibbs free energy produces eq 13 and 14:

$$\Delta G^\circ = -RT\ln k_l = \Delta H^\circ - T\Delta S^\circ \quad (13)$$

$$\ln k_l = \frac{\Delta S}{R} - \frac{\Delta H}{RT} \quad (14)$$

The parameters can be evaluated using a Van't Hoff plot (Figure 11), which illustrates the relationship between adsorption and temperature of RB5 and RO16. Plotting 1/T vs ln(k_l).

The gradient of the regression line from the Van't Hoff plot can be used to calculate ΔH and the intercept is used to calculate ΔS. The thermodynamic parameters for RB5 and RO16 are detailed in Table 5. The data in Table 5 indicates that for all temperatures investigated, adsorption is a spontaneous process, as evidenced by the negative ΔG value for temperatures 10-40°C. This data is in agreement with previously published findings regarding dye adsorption onto LDH/MMO adsorbents [18, 24]. The ΔH values for RB5 (-102.33 kJ mol^{-1}) and RO16 (-56.07 kJ mol^{-1}) indicate that the adsorption process was exothermic in nature which is supported by the data relating to the isotherms, which illustrates reduced q_m with increasing temperature. The enthalpy values also indicate that the process was primarily chemisorption rather than physisorption, occurring as a result of the electrostatic attractions between the R-SO_3^- functional groups and the regenerated brucite-like layers, which further supports the idea that the LDH is adsorbing the dye molecules through intercalation into the interlayer region of the LDH as seen in previous literature [18, 47]. The negative entropy suggests a reduction in freedom of the adsorbent-adsorbate interactions at the surface of the adsorbent, however as the exothermic reaction progresses the entropy of the overall system would increase. The data regarding both enthalpy and entropy is contradictory with much of the published literature regarding dye adsorption onto MMO and LDH based adsorbents, in which many of the processes are found to be endothermic in nature with positive ΔS also [18, 24, 47-49].

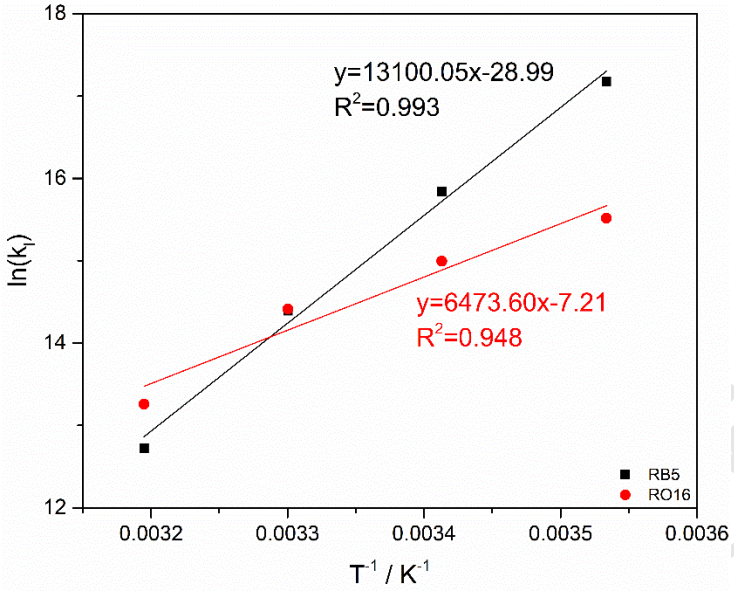

Figure 11 Van't Hoff plot for adsorption of Reactive Black 5 (RB5) and Reactive Orange 16 (RO16) from simulated wastewater

Table 5 Thermodynamic parameters of Reactive Black 5 (RB5) and Reactive Orange 16 (RO16) adsorption

ΔH / kJ mol^{-1}	ΔS / kJ K^{-1} mol^{-1}	ΔG / kJ mol^{-1}			
RB5		10°C	20°C	30°C	40°C
-102.33	-0.22	-40.21	-38.01	-35.82	-33.62
RO16		10°C	20°C	30°C	40°C
-56.07	-0.06	-39.11	-38.51	-37.91	-37.31

3.9. Effect of Coexisting Anionic Compounds

Electrolyte salts and alkaline chemicals are added to dye baths to enhance diffusion of dye through the substrate and to enhance fixation [3]. These additives will be present in the dye bath effluent and so investigating their effects on the adsorption of dyes is essential. Increasing Na_2CO_3 and Na_2SO_4 content, even to 1 g L^{-1}, results in a reduction in

adsorption capacity of both RB5 and RO16 (Figure 12). The charge density of CO_3^{2-} and SO_4^{2-} ions outweigh that of the adsorbate dye molecules, in accordance with previously reported literature, the fact that SO_4^{2-} has less of an impact on adsorption compared with CO_3^{2-} is in accordance with previously reported results by Parker *et al.* [50]. Na_2SO_4 causes a reduction in concentration of RB5 of 6±2% with 10 g L^{-1} compared with 7±2% for Na_2CO_3. Regardless of the amount of Cl^- added the reduction in concentration remains at approximately 37%. The reduction of RO16 concentration for the carbonate and sulfate additives is more polarised, with Na_2CO_3 resulting in a near complete inhibition of dye removal at 10 g L^{-1}, whereas sodium sulfate results in 34±3% reduction in RO16 at 10 g L^{-1}. The presence of NaCl in solution appears to have little impact on adsorption suggesting that Cl^- do not present a large enough charge density to impact adsorption of RO16 and reduction in concentration remains between 55-60%. The reduction in capacity as a result of CO_3^{2-} and SO_4^{2-} presence is of concern as the presence of alkaline carbonates is common in the fixation of dyes and additional adsorbent would be required to remove the carbonate due to the high specificity of MMO/CO_3^{2-} interactions.

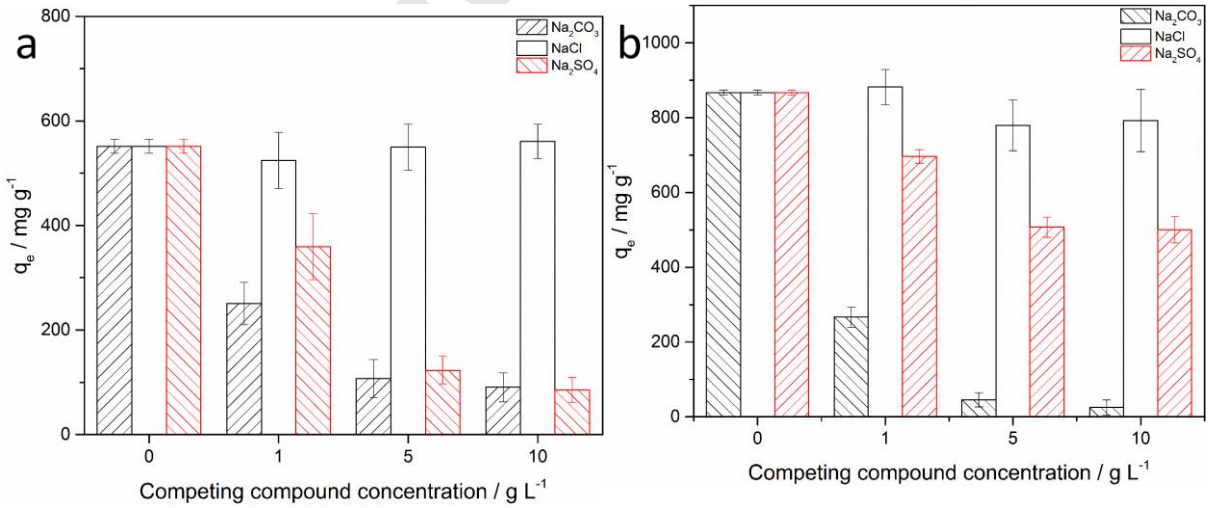

Figure 12 Effect of competing anions on adsorption of a) Reactive Black 5 b) Reactive Orange 16

3.10. Adsorbent Regeneration

Regeneration and subsequent capacity is one of the key aspects in the choice of adsorbent, as poor regenerative capacity will reduce the lifetime effectiveness of adsorption media [51]. Thermal regeneration via calcination was conducted at 500°C because the MMO was initially generated by thermal degradation of the LDH at 500°C. Thermogravimetric analysis indicated that there is a breakdown of the layered structure above 400°C, however thermal generation, and regeneration, at temperatures above 600°C starts to produce spinel structures which cannot reform LDH structures and the adsorption capacity is reduced [30, 31].

The simple thermal regeneration resulted in q_e being reduced from 560±11 mg g^{-1} to 24±35 mg g^{-1} after the first cycle (Figure 13). The adsorption capacity at equilibrium is effectively reduced to almost nothing by the fourth cycle, where q_e is 1±10 mg g^{-1}. In an effort to mitigate the poor regeneration of the MMO/LDH adsorbent, an extra step of CO_3^{2-} ion exchange was implemented prior to thermal regeneration. Washing the spend MMO adsorbent with Na_2CO_3 resulted in an increase in adsorption capacity compared with simply thermally regenerating the MMO. The q_e after cycle four was 102±1 mg g^{-1}, reduced from 566±19mg g^{-1} during the first adsorption experiment (Figure 13). The reduced uptake is attributed to thermal degradation products of the adsorbed dye. Upon heating the spent MMO adsorbent thermal decomposition products from the RB5 dye, some carbonaceous material and residual sulfur are left in the MMO matrix [24]. Elemental analysis of fresh MMO and material recovered from thermal regeneration indicates that there is sulfur present in the regenerated material (Figure 14). The sulfur present is likely to impact on adsorption capacity by blocking the active sites and reducing the available space for subsequent adsorption. The reduced adsorption capacity in spite of CO_3^{2-} washing is attributed to not achieving complete ion exchange between the $R\text{-}SO_3^-$

and CO_3^{2-} functional groups in the washing stage. The slow adsorption kinetics of the dye during LDH reformation may be indicative of longer washing times needed compared with what was used (2 hours). Some other research investigations have however found that regeneration of LDH/MMO adsorbents yields high adsorption for more than one adsorption cycle [52, 53]. The work by Chen *et al.* is carried out using a composite Fe_3O_4@MgAl-CO_3 composite and Congo red dye with catalysed advanced oxidation, to regenerate the MMO [52]. This is a key area of research that will need to be investigated if LDHs are to serve as a useful and sustainable adsorbent.

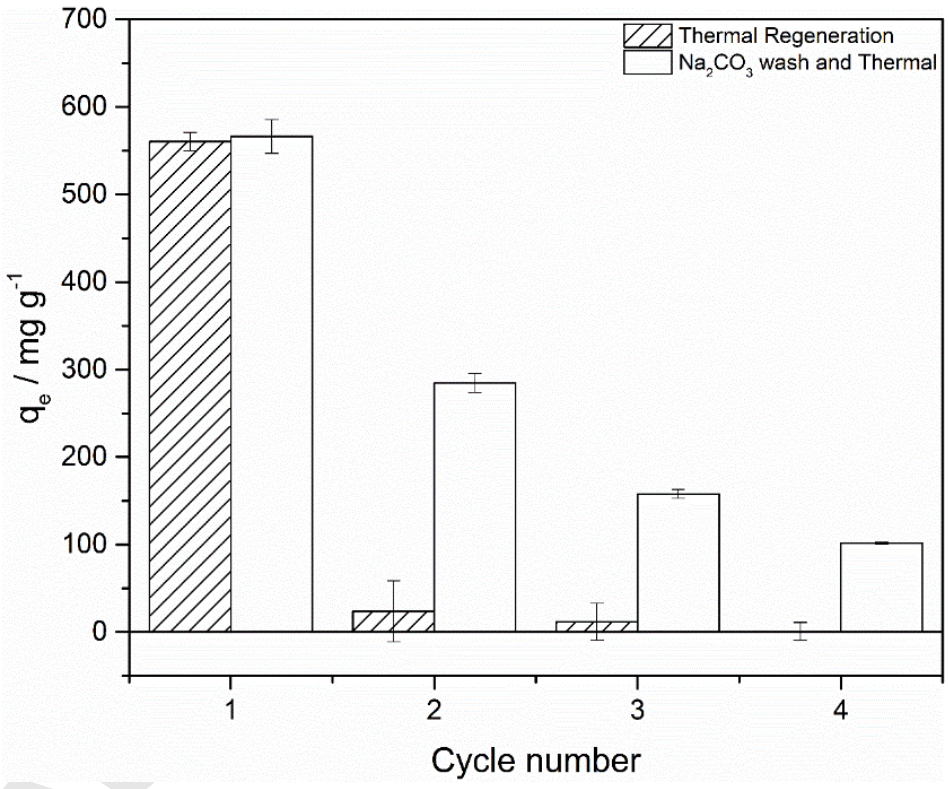

Figure 13 Reactive Black 5 adsorption after thermal regeneration

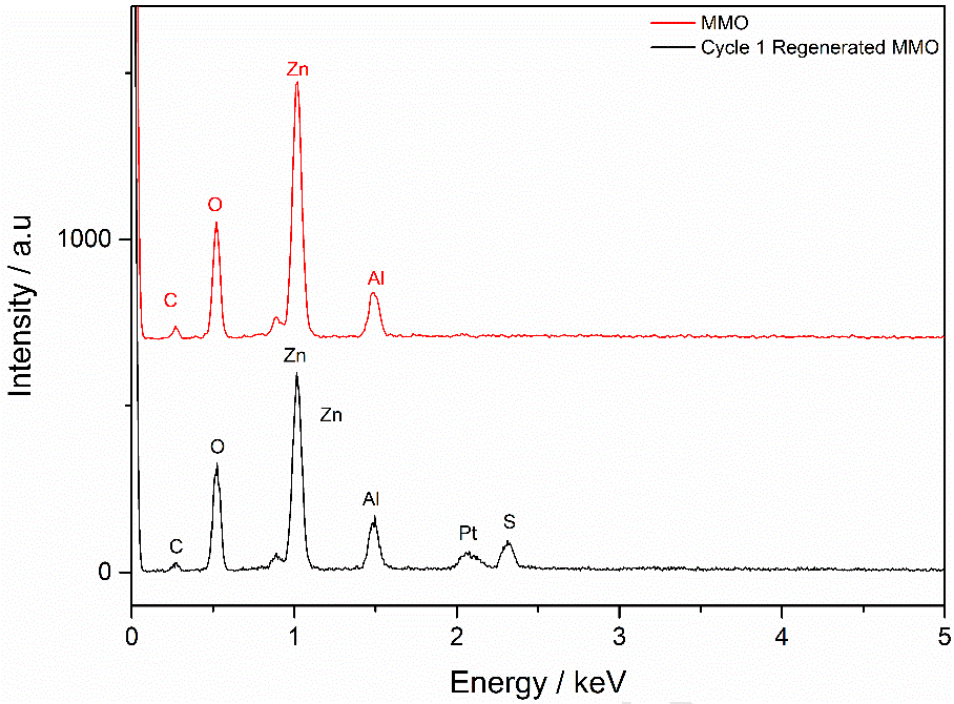

Figure 14 Energy dispersive X-ray spectra of calcined Zn_2Al-CO_3 (MMO) and Zn_2Al after dye adsorption (note trace contamination of Pt, possibly introduced during sintering)

3.11. Proposed Adsorption Mechanism

The primary method of adsorption is the regeneration of LDH platelets and intercalation of dye molecules into the interlayer region. This is evident from the shift to lower Bragg angle of the most intense reflections in the LDH diffractograms in Figure 15. The diffractogram for the fresh LDH, also seen in Figure 2, has an intense reflection at 11.5° 2θ relating to the d_{003} basal spacing, whereas this reflection has shifted to 4.5° and 3.1° for the RB5 and RO16 regenerated samples respectively. This shift in basal spacing is due to the greater molecular weight and size of the dye molecules compared to CO_3^{2-} ions present in the fresh LDH. The basal spacing for the RB5 and RO16 adsorbed samples was calculated as 1.9 nm and 2.8 nm respectively. Figure 13 shows a proposed schematic of RB5 adsorption. There are also some minor reflections relating to the d_{003} basal spacing of CO_3^{2-} intercalated LDHs in

Figure 15. The Zn_2Al-CO_3 reflections suggest that without complete decarbonation of the water and a CO_2 free atmosphere CO_3^{2-} ions will intercalate as a result of residual CO_3^{2-} in the water and the alkaline buffering effect of LDH layers dissolving CO_2 from the atmosphere [27].

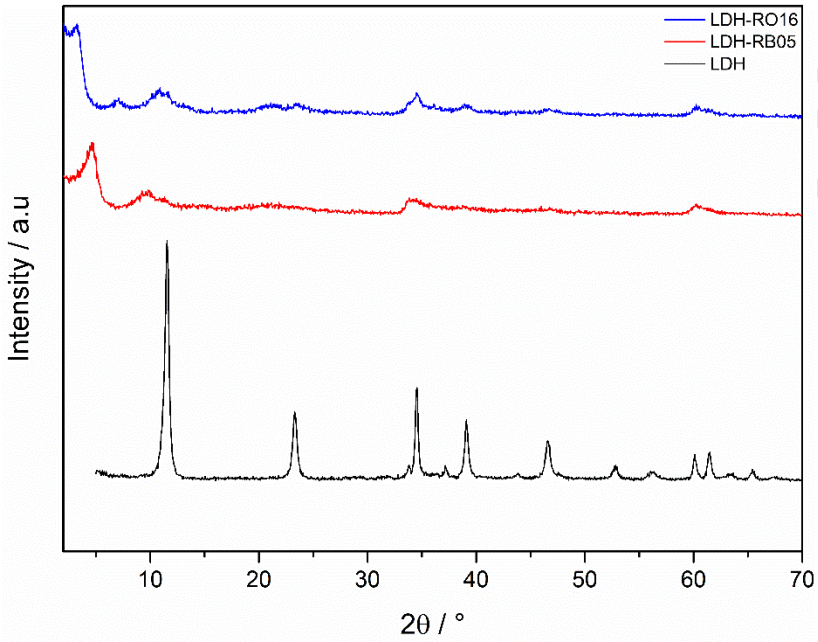

Figure 15 X-ray diffractograms of Fresh LDH and exhausted LDH following RB5 and RO16 adsorption at 20°C

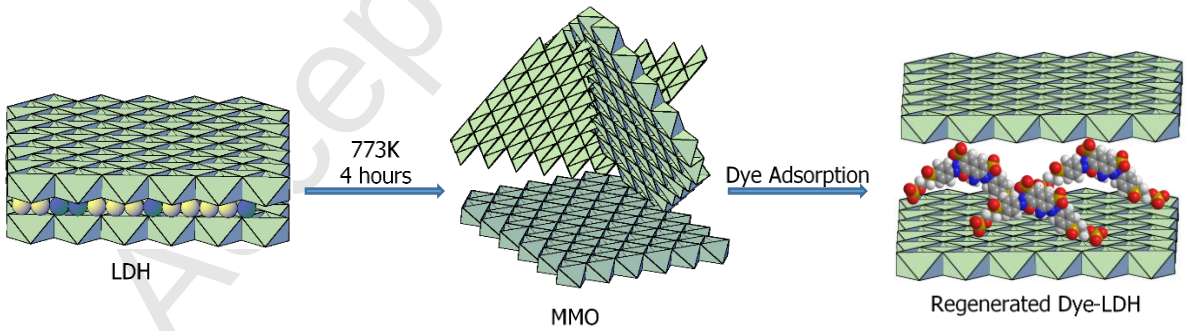

Figure 16 Adsorption schematic illustrating the memory effect

4. Conclusions

The inherent stability of synthetic dyes makes their removal from waste water more difficult than many other types of organic contaminant. Layered Double Hydroxides have shown great potential in literature due to their ability to adsorb large quantities of dye through the *memory effect*.

In this work, large scale continuous synthesis of $Zn_2Al\text{-}CO_3$ LDHs alongside adsorption of dyes Reactive Black 5 and Reactive Orange 16 were investigated to determine the effectiveness of large scale production and application of LDHs as precursors for adsorbents.

The adsorption capacity of RO16 (q_m=895 mg g^{-1}) was greater than RB5 (589 mg g^{-1}). This was due to the size of the dye molecules and the increased number of $R\text{-}SO_3^-$ functional groups present in RB5 occupying adsorbent active sites. The larger size of RB5 also sterically hinders the adsorbate from interacting with adsorbent surface. Competing anions were investigated along with a range of pH values which may be found in commercial dyebath effluent. Initial pH was found to have little impact on adsorption of both RB5 and RO16. The addition of Na_2CO_3 and Na_2SO_4 reduced adsorption, while the addition of NaCl resulted in no change in q_e. Adsorption capacity was reduced after the first adsorption-regeneration cycle and continued to reduce with subsequent cycles.

Zn_2AlCO_3 has a high adsorption capacity for RB5 and RO16 as well as regeneration potential, which suggests that LDHs may have a real-world application for the remediation of dyes from wastewater. The uptake capacity of the MMO adsorbent, and continuous synthesis ensures a rapid controlled scalable process for adsorption reactions of reactive dyebath effluents with high concentrations of synthetic dyes.

5. Acknowledgements

The authors would like to acknowledge and thank the EPSRC for providing scholarship funding through the University of Nottingham (EP/M5065881/1). Our thanks to the staff at Promethean Particles Ltd for assistance throughout the synthesis of materials at pilot scale. This work was part funded by the European Union's Seventh Framework Programme (FP7/2007–2013), grant agreement no. FP7-NMP4-LA-2012-280983, SHYMAN. We would also like to express our gratitude to Rhys William Lodge and the Nottingham Nanoscale and Microscale Research Centre, for access to electron microscopes used for this work.

6. References

[1] M. Clark, Handbook of Textile and Industrial Dyeing, Volume 1 - Principles, Processes and Types of Dyes, Woodhead Publishing.
[2] M. Bide, Dyeing, Kirk-Othmer Encyclopedia of Chemical Technology, John Wiley & Sons, Inc.2000.
[3] R.M. Christie, Colour Chemistry (2nd Edition), 2 ed., Royal Society of Chemistry2015.
[4] M. Clark, Handbook of Textile and Industrial Dyeing, Volume 2 - Applications of Dyes, Woodhead Publishing.
[5] J. Binkley, A. Kandelbauer, 6 - Effluent treatment – Enzymes in activated sludge, Textile Processing with Enzymes, Woodhead Publishing2003, pp. 199-221.
[6] S.M. Auerbach, K.A. Carrado, P.K. Dutta, Handbook of layered materials, M. Dekker, New York, 2004.
[7] F. Cavani, F. Trifiro, A. Vaccari, Hydrotalcite-type Anionic Clays: Preparation, Properties and Applications, Catalysis Today 11(2) (1991) 173-301.
[8] X. Duan, D.G. Evans, Layered double hydroxides, Springer, Berlin ; New York, 2006.
[9] R. Xu, W. Pang, Q. Huo, Modern Inorganic Synthetic Chemistry, Modern Inorganic Synthetic Chemistry (2011) 1-590.
[10] G.B. Sun, L.N. Sun, H. Wen, Z.Q. Jia, K.L. Huang, C.W. Hu, From layered double hydroxide to spinel nanostructures: Facile synthesis and characterization of nanoplatelets and nanorods, Journal of Physical Chemistry B 110(27) (2006) 13375-13380.
[11] T. Hongo, T. Iemura, A. Yamazaki, Adsorption ability for several harmful anions and thermal behavior of Zn-Fe layered double hydroxide, Journal of the Ceramic Society of Japan 116(1350) (2008) 192-197.
[12] H.N.N. Ha, N.T.K. Phuong, T.B. An, N.T.M. Tho, T.N. Thang, B.Q. Minh, C.V. Du, Arsenate removal by layered double hydroxides embedded into spherical polymer beads: Batch and column studies, J. Environ. Sci. Health Part A-Toxic/Hazard. Subst. Environ. Eng. 51(5) (2016) 403-413.

[13] K. Grover, S. Komarneni, H. Katsuki, Synthetic hydrotalcite-type and hydrocalumite-type layered double hydroxides for arsenate uptake, Applied Clay Science 48(4) (2010) 631-637.
[14] L.C. Hsu, S.L. Wang, Y.M. Tzou, C.F. Lin, J.H. Chen, The removal and recovery of Cr(VI) by Li/Al layered double hydroxide (LDH), Journal of Hazardous Materials 142(1-2) (2007) 242-249.
[15] L.H. Ai, C.Y. Zhang, L.Y. Meng, Adsorption of Methyl Orange from Aqueous Solution on Hydrothermal Synthesized Mg-Al Layered Double Hydroxide, Journal of Chemical and Engineering Data 56(11) (2011) 4217-4225.
[16] U. Costantino, N. Coletti, M. Nocchetti, G.G. Aloisi, F. Elisei, Anion exchange of methyl orange into Zn-Al synthetic hydrotalcite and photophysical characterization of the intercalates obtained, Langmuir 15(13) (1999) 4454-4460.
[17] C. Peng, J. Dai, J.Y. Yu, J. Yin, Calcined Mg-Fe layered double hydroxide as an absorber for the removal of methyl orange, Aip Advances 5(5) (2015).
[18] H. Zaghouane-Boudiaf, M. Boutahala, L. Arab, Removal of methyl orange from aqueous solution by uncalcined and calcined MgNiAl layered double hydroxides (LDHs), Chemical Engineering Journal 187 (2012) 142-149.
[19] A.R. Auxilio, P.C. Andrews, P.C. Junk, L. Spiccia, D. Neumann, W. Raverty, N. Vanderhoek, Adsorption and intercalation of Acid Blue 9 on Mg-Al layered double hydroxides of variable metal composition, Polyhedron 26(14) (2007) 3479-3490.
[20] C. Zhang, S.G. Yang, H.Z. Chen, H. He, C. Sun, Adsorption behavior and mechanism of reactive brilliant red X-3B in aqueous solution over three kinds of hydrotalcite-like LDHs, Applied Surface Science 301 (2014) 329-337.
[21] H. Abdolmohammad-Zadeh, E. Ghorbani, Z. Talleb, Zinc-aluminum layered double hydroxide as a nano-sorbent for removal of Reactive Yellow 84 dye from textile wastewater effluents, Journal of the Iranian Chemical Society 10(6) (2013) 1103-1112.
[22] T.P.F. Teixeira, S.I. Pereira, S.F. Aquino, A. Dias, Calcined Layered Double Hydroxides for Decolorization of Azo Dye Solutions: Equilibrium, Kinetics, and Recycling Studies, Environmental Engineering Science 29(7) (2012) 685-692.
[23] I. Clark, P.W. Dunne, R.L. Gomes, E. Lester, Continuous hydrothermal synthesis of Ca2Al-NO3 layered double hydroxides: The impact of reactor temperature, pressure and NaOH concentration on crystal characteristics, Journal of Colloid and Interface Science 504 (2017) 492-499.
[24] Y.W. Guo, Z.L. Zhu, Y.L. Qiu, J.F. Zhao, Enhanced adsorption of acid brown 14 dye on calcined Mg/Fe layered double hydroxide with memory effect, Chemical Engineering Journal 219 (2013) 69-77.
[25] Q. Wang, S. Tang, E. Lester, D. O'Hare, Synthesis of ultrafine layered double hydroxide (LDHs) nanoplates using a continuous-flow hydrothermal reactor, Nanoscale 5(1) (2013) 114-117.
[26] S.C.B. Abrahams, J.L.;, Remeasurement of the Structure of Hexagonal ZnO, Acta Crystallographica 25 (1969).
[27] K. Livansky, EFFECT OF TEMPERATURE AND PH ON ABSORPTION OF CARBON-DIOXIDE BY A FREE LEVEL OF MIXED-SOLUTIONS OF SOME BUFFERS, Folia Microbiologica 27(1) (1982) 55-59.
[28] M. Thommes, K. Kaneko, A.V. Neimark, J.P. Olivier, F. Rodriguez-Reinoso, J. Rouquerol, K.S.W. Sing, Physisorption of gases, with special reference to the evaluation of surface area and pore size distribution (IUPAC Technical Report), Pure and Applied Chemistry 87(9-10) (2015) 1051-1069.
[29] J. Das, B.S. Patra, N. Baliarsingh, K.M. Parida, Adsorption of phosphate by layered double hydroxides in aqueous solutions, Applied Clay Science 32(3-4) (2006) 252-260.
[30] L. Lv, J. He, M. Wei, D.G. Evans, X. Duan, Factors influencing the removal of fluoride from aqueous solution by calcined Mg-Al-CO3 layered double hydroxides, Journal of Hazardous Materials 133(1-3) (2006) 119-128.
[31] S. Mandal, S. Mayadevi, Adsorption of fluoride ions by Zn-Al layered double hydroxides, Applied Clay Science 40(1-4) (2008) 54-62.
[32] H.A. Hamid, Y. Jenidi, W. Thielemans, C. Somerfield, R.L. Gomes, Predicting the capability of carboxylated cellulose nanowhiskers for the remediation of copper from water using response

surface methodology (RSM) and artificial neural network (ANN) models, Industrial Crops and Products 93 (2016) 108-120.
[33] J. Orthman, H.Y. Zhu, G.Q. Lu, Use of anion clay hydrotalcite to remove coloured organics from aqueous solutions, Separation and Purification Technology 31(1) (2003) 53-59.
[34] P. Pengthamkeerati, T. Satapanajaru, O. Singchan, Sorption of reactive dye from aqueous solution on biomass fly ash, Journal of Hazardous Materials 153(3) (2008) 1149-1156.
[35] M.S. Tanyildizi, Modeling of adsorption isotherms and kinetics of reactive dye from aqueous solution by peanut hull, Chemical Engineering Journal 168(3) (2011) 1234-1240.
[36] R. Patel, S. Suresh, Kinetic and equilibrium studies on the biosorption of reactive black 5 dye by Aspergillus foetidus, Bioresource Technology 99(1) (2008) 51-58.
[37] K. Vijayaraghavan, Y.S. Yun, Biosorption of C.I. Reactive Black 5 from aqueous solution using acid-treated biomass of brown seaweed Laminaria sp, Dyes and Pigments 76(3) (2008) 726-732.
[38] Z. Aksu, S. Tezer, Biosorption of reactive dyes on the green alga Chlorella vulgaris, Process Biochemistry 40(3-4) (2005) 1347-1361.
[39] O. Ozdemir, B. Armagan, M. Turan, M.S. Celik, Comparison of the adsorption characteristics of azo-reactive dyes on mezoporous minerals, Dyes and Pigments 62(1) (2004) 49-60.
[40] Z. Eren, F.N. Acar, Adsorption of Reactive Black 5 from an aqueous solution: equilibrium and kinetic studies, Desalination 194(1-3) (2006) 1-10.
[41] E. Guibal, E. Touraud, J. Roussy, Chitosan interactions with metal ions and dyes: Dissolved-state vs. solid-state application, World Journal of Microbiology & Biotechnology 21(6-7) (2005) 913-920.
[42] V.K. Gupta, B. Gupta, A. Rastogi, S. Agarwal, A. Nayak, A comparative investigation on adsorption performances of mesoporous activated carbon prepared from waste rubber tire and activated carbon for a hazardous azo dye-Acid Blue 113, Journal of Hazardous Materials 186(1) (2011) 891-901.
[43] Y.S. Ho, G. McKay, Pseudo-second order model for sorption processes, Process Biochemistry 34(5) (1999) 451-465.
[44] N. Kannan, M.M. Sundaram, Kinetics and mechanism of removal of methylene blue by adsorption on various carbons - a comparative study, Dyes and Pigments 51(1) (2001) 25-40.
[45] J.B. Zhou, S.L. Yang, J.G. Yu, Z. Shu, Novel hollow microspheres of hierarchical zinc-aluminum layered double hydroxides and their enhanced adsorption capacity for phosphate in water, Journal of Hazardous Materials 192(3) (2011) 1114-1121.
[46] C.S. Lei, M. Pi, P.Y. Kuang, Y.Q. Guo, F.G. Zhang, Organic dye removal from aqueous solutions by hierarchical calcined Ni-Fe layered double hydroxide: Isotherm, kinetic and mechanism studies, Journal of Colloid and Interface Science 496 (2017) 158-166.
[47] R. Extremera, I. Pavlovic, M.R. Perez, C. Barriga, Removal of acid orange 10 by calcined Mg/Al layered double hydroxides from water and recovery of the adsorbed dye, Chemical Engineering Journal 213 (2012) 392-400.
[48] J.C. Huang, C.Y. Kuo, C.H. Wu, Y.H. Lin, Adsorption of CI Reactive Red 2 by ZnAl-layered double hydroxides: kinetics, equilibrium, and thermodynamics, Desalination and Water Treatment 70 (2017) 372-379.
[49] W.Y. Huang, X. Yu, D. Li, Adsorption removal of Congo red over flower-like porous microspheres derived from Ni/Al layered double hydroxide, Rsc Advances 5(103) (2015) 84937-84946.
[50] L.M. Parker, N.B. Milestone, R.H. Newman, THE USE OF HYDROTALCITE AS AN ANION ABSORBENT, Industrial & Engineering Chemistry Research 34(4) (1995) 1196-1202.
[51] G. Tchobanoglous, H.D. Stensel, R. Tsuchihashi, F.L. Burton, M. Abu-Orf, G. Bowden, W. Pfrang, Metcalf & Eddy, Wastewater engineering : treatment and resource recovery, Fifth edition / ed., McGraw-Hill Education, New York, NY, 2014.

[52] C.P. Chen, P. Gunawan, R. Xu, Self-assembled Fe3O4-layered double hydroxide colloidal nanohybrids with excellent performance for treatment of organic dyes in water, Journal of Materials Chemistry 21(4) (2011) 1218-1225.
[53] Z.M. Ni, S.J. Xia, L.G. Wang, F.F. Xing, G.X. Pan, Treatment of methyl orange by calcined layered double hydroxides in aqueous solution: Adsorption property and kinetic studies, Journal of Colloid and Interface Science 316(2) (2007) 284-291.